Structural Eng./Earthquake Eng., JSCE, Vol. 19, No. 2 [Special Issue], 169s—178s, 2002 October

NON-LINEAR STATIC MODELING OF DIP-SLIP FAULTS FOR STUDYING GROUND SURFACE DEFORMATION USING APPLIED ELEMENT METHOD

Pradeep K. RAMANCHARLA[1] and Kimiro MEGURO[2]

[1] Ph.D. Student, Institute of Industrial Science, The University of Tokyo
[2] Dr. of Eng., Associate Prof., International Center for Disaster-Mitigation Engineering (INCEDE), Institute of Industrial Science, The University of Tokyo

Earthquakes in different geological regions show drastic variations in their effects such as, large surface upliftment/displacements of unconsolidated soil deposits. For this reason, we attempted to develop a new application of Applied Element Method (AEM) to study the ground surface deformation near fault rupture zone. First, preliminary analysis is carried out to check the applicability of the method. Results are compared with the results from analytical and experimental methods and they showed good agreement. Non-linear modeling is carried out to study the effects of dip-slip faults on the ground surface. Detailed study is carried out using two cases of dip angles in both normal and reverse dip-slip fault conditions.

Key Words: *Applied Element Method, AEM, active fault, dip-slip fault, surface rupture, Ji-Ji earthquake, Kocaeli earthquake*

1. INTRODUCTION

Two enormously disastrous earthquakes hit the globe in 1999. The first one was an earthquake of magnitude 7.4 (Mw) occurred in Turkey on 17th August 1999[1)], and immediately following that, another event of magnitude 7.3 (Mw, Central Weather Bureau, Taiwan) occurred in Taiwan on 21st September 1999[2)]. Both events caused immense loss to property and lives. The earthquake fault (North Anatolian Fault) in Turkey was traced over 100 km. The magnitude of right lateral movement of the fault on the ground surface was measured to be 2 to 4 m. Normal faults, which were caused secondarily, sunk huge area by a depth of 2-3 m. And in Taiwan, severer effects were observed. The earthquake fault (Cher-Lung-Pu Fault) was traced for about 80 km, here the fault movement directly caused severe damage. The magnitude of maximum vertical differential movement was measured to be nearly 10.0 m as shown in **Fig. 1**. Though these earthquakes were tragic, also provided us the momentum to the process of improvement in understanding the behavior of nature. From the above two events, it is clear that the severe damage can be caused not only by the strong ground motion but also due to large surface deformations lying directly over the seismic faults. Hence, it is necessary to direct our efforts to study the relation between seismic fault characteristics, thickness of soil deposit and surface deformation. Many researchers conducted experiments to understand the phenomena of surface failure, Cole and Lade[3)] have tried to determine the location of surface fault rupture and width of the affected zone in alluvium over dip-slip fault using fault test box. Lade et al.[4)] studied to determine the multiple failure surfaces by conducting the experiments on sand using fault test

Fig. 1 About 10 m vertical displacement is seen at the Shih-Kang dam site, Taiwan

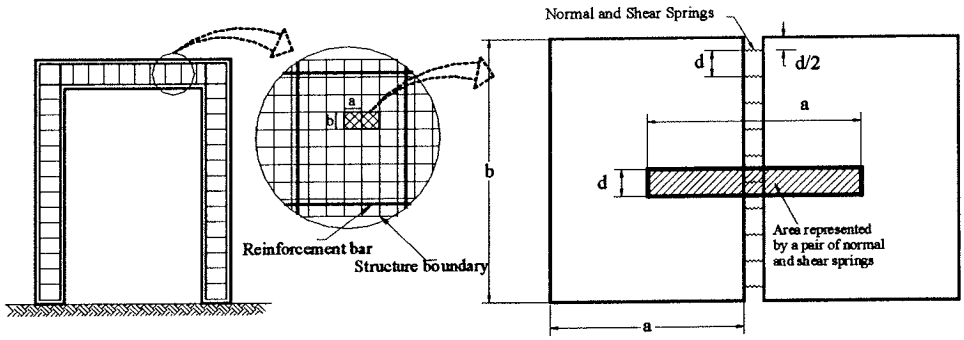

(a) Element generation for AEM

(b) Spring distribution and area of influence of each pair of springs

Fig. 2 Modelling of structure to AEM

box. Onizuka et al.[5] have modelled the deformation of ground using aluminium rods. Through experiments, they investigated bedrock stresses induced by reverse dip-slip faults. Using the above experimental methods, we can find the influence length. However, replicating the actual field conditions using experiments is very difficult, especially, controlling the material properties and modelling the boundary conditions. Moreover, large amount of data is necessary to establish a relationship between seismic fault parameters and resulting surface deformation. On the other hand, studying this phenomenon using numerical model has the advantage of controlling the parameters like material properties, size of the model, boundary condition, dip angle, etc.

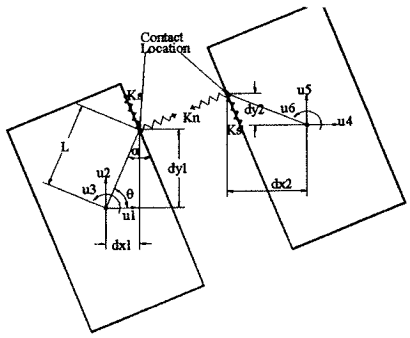

Fig. 3 Spring connectivity

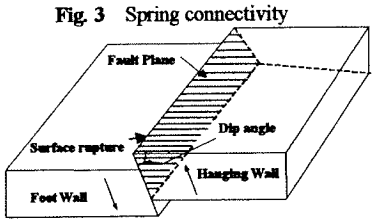

Fig. 4 Fault terminology

2. ELEMENT FORMULATION

With the AEM [6)~8)], structure is modelled as an assembly of small elements that are made by dividing of the structure virtually, as shown in **Fig. 2 (a)**. The two elements shown in **Fig. 2(b)** are assumed to be connected by pairs of normal and shear springs located at contact locations that are distributed around the element edges. Each pair of springs totally represents stresses and deformations of a certain area (hatched area in **Fig. 2 (b)**) of the studied elements. The spring stiffness is determined as shown in **Eq. (1)**:

$$K_n = \frac{E \times d \times T}{a} \text{ and } K_s = \frac{G \times d \times T}{a} \qquad (1)$$

where, d is the distance between springs, T is the thickness of the element and "a" is the length of the representative area, E and G are the Young's and shear modulus of the material, respectively. The above equation indicates that each spring represents

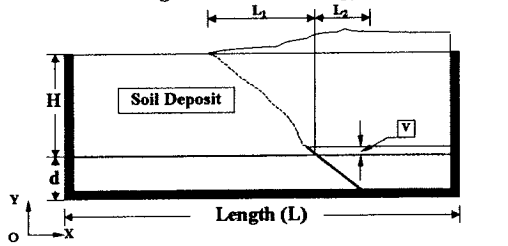

(a) Fault model

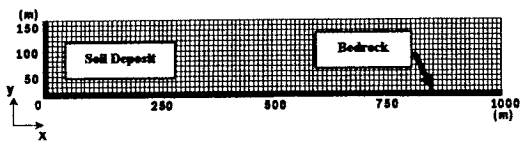

Fig. 5 (b) Numerical model

the stiffness of an area (d x T) with length "a" of the studied material. In case of reinforcement, this area is replaced by that of the reinforcement bar. The above equation indicates that the spring stiffness is calculated as if the spring connects the element centerlines.

Three degrees of freedom are assumed for each element. These degrees of freedom represent the rigid body motion of the element. Although the element motion is a rigid body motion, its internal stress and deformations can be calculated by the spring deformation around each element. This means that although the element shape doesn't change during analysis, the behavior of assembly of elements is deformable.

The two elements shown in **Fig. 3** are assumed to be connected by only one pair of normal (stiffness: Kn) and shear (stiffness: Ks) springs. The values of (dx and dy) correspond to the relative coordinate of the contact point with respect to the centroid. To have a general stiffness matrix, the location of element and contact springs are assumed in a general position. The stiffness matrix components corresponding to each degree of freedom are determined by assuming a unit displacement in the studied direction and by determining forces at the centroid of each element. The element stiffness matrix size is only (6 x 6). Equation (2) shows the components of the upper left quarter of the stiffness matrix. All used notations in this equation are shown in **Fig. 3**. It is clear that the stiffness matrix depends on the contact spring stiffness and the spring location. For more details, please refer ref. 7.

$$\begin{bmatrix} \sin^2(\theta+\alpha)K_n + \cos^2(\theta+\alpha)K_s & -K_n\sin(\theta+\alpha)\cos(\theta+\alpha) + K_s\sin(\theta+\alpha)\cos(\theta+\alpha) & \cos(\theta+\alpha)K_sL\sin(\alpha) - \sin(\theta+\alpha)K_nL\cos(\alpha) \\ -K_n\sin(\theta+\alpha)\cos(\theta+\alpha) + K_s\sin(\theta+\alpha)\cos(\theta+\alpha) & \sin^2(\theta+\alpha)K_s + \cos^2(\theta+\alpha)K_n & \cos(\theta+\alpha)K_nL\cos(\alpha) + \sin(\theta+\alpha)K_sL\sin(\alpha) \\ \cos(\theta+\alpha)K_sL\sin(\alpha) - \sin(\theta+\alpha)K_nL\cos(\alpha) & \cos(\theta+\alpha)K_nL\cos(\alpha) + \sin(\theta+\alpha)K_sL\sin(\alpha) & L^2\cos^2(\alpha)K_n + L^2\sin^2(\alpha)K_s \end{bmatrix} \quad (2)$$

The stiffness matrix in Eq. (2) is for only one pair of contact springs. However, the global stiffness matrix is determined by summing up the stiffness matrices of individual pair of springs around each element. Consequently, the developed stiffness matrix is an average stiffness matrix for the element according to the stress situation around the element. This technique can be used both in load and displacement control cases. The governing equation is

$$[K_G][\Delta] = [F] \quad (3)$$

where, $[K_G]$ is the global stiffness matrix; $[\Delta]$ the displacement vector and $[F]$ the applied load vector. In load control case, the vector, $[F]$, is known before the analysis. In displacement control case, the load is applied by unit virtual displacement for one or more degrees of freedom. By using the advantage of AEM's simplicity in formulation and accuracy in non-linear range, fault rupture zone shown in **Fig. 4** is modelled.

The mechanism shown in **Fig. 4** is called Reverse Dip-Slip Faulting. This is one of the types of faults where the hanging wall moves upward relative to the footwall. If the direction of the movement of the hanging wall is downward then it is called normal faulting. In the study discussed in this paper, both normal and reverse dip-slip faults are considered. To analyse the mechanism of fault rupture zone near dip-slip faults, the model shown in **Fig. 5 (a)** was prepared. In this numerical model, soil deposit of thickness, H (=140 m), is assumed to be overlay on the bedrock. The length of the model, L, is assumed as 1,000 m **(Fig. 5 (b))**. Influence lengths (affected area), L_1 and L_2, in **Fig. 5 (a)**, on the surface towards left and right side from the point exactly above the seismic fault, respectively, are calculated by giving the hanging wall a displacement along the direction of dip angle. Whole deposit is discritized into 1500 square shaped elements each of size 10x10 m.

3. BOUNDARY CONDITION

Generally, soil strata and bedrock extend upto tens of kilometers in horizontal direction. Numerical modeling of such a large media is a difficult task and moreover, for studying the surface behavior near the active fault region, it is necessary to model the small portion of the region that will include all the effects when the bedrock moves. For studying the selected region numerically, we need to assume an appropriate boundary condition such that it will not affect the numerical results greatly. Since the present formulation is done for static case, we assume the boundary on left side to be fixed in horizontal direction, and free to move in vertical direction and can rotate. In order to avoid the interference of boundary condition on numerical results, left side boundary is kept at sufficient distance from the fault zone. The Bottom of the bedrock is assumed as fixed. We think that this kind of boundary condition is appropriate for this problem because more emphasis is given to the near fault behavior of the formulated model. In case of dynamics, modeling of radiation condition is very important and the boundary condition discussed here can be easily replaced by viscous boundary condition or transmitting boundary[9].

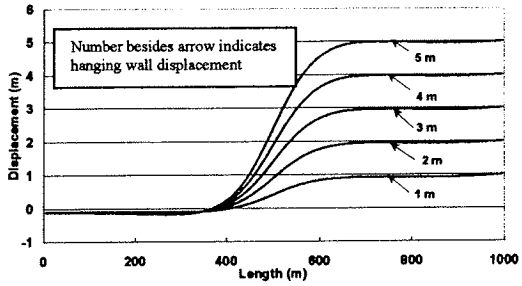

(a) Surface displacement

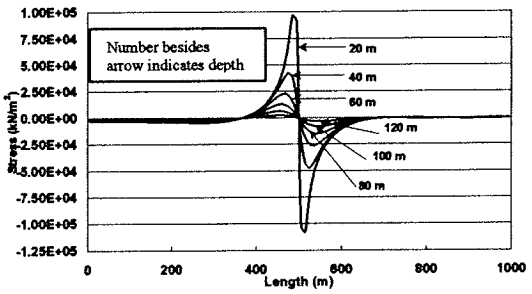

(b) Normal stresses in soil deposit at regular intervals

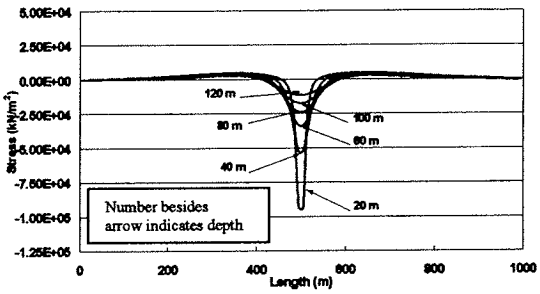

(c) Shear stresses in soil deposit at regular intervals

Fig. 6 Analysis results for Case 1

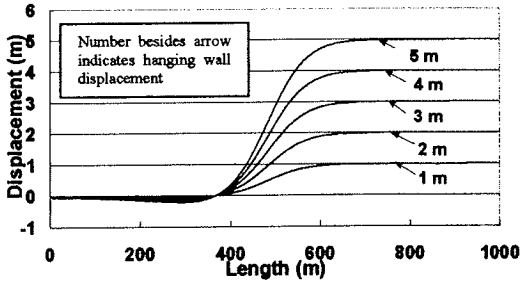

(a) Surface displacement

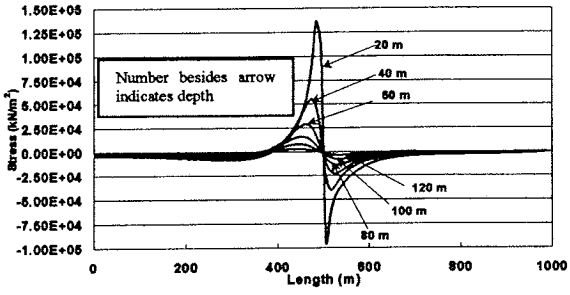

(b) Normal stresses in soil deposit at regular intervals

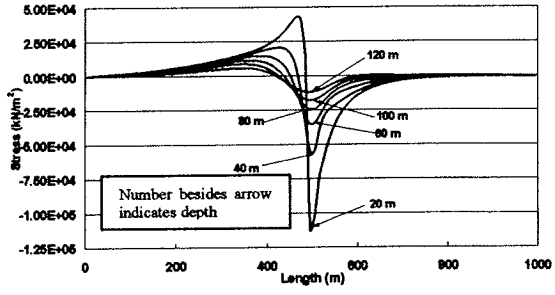

(c) Shear stresses in soil deposit at regular intervals

Fig. 7 Analysis results for Case 2

4. ELASTIC ANALYSIS

To verify the proposed model, analysis is carried out in elastic case (see **Table 1**. for description of analysis) by assuming two different dip angles. In Case 1, dip angle is assumed as 90^0 and in Case 2, it is assumed as 45^0. Density and Young's modulus, E, shear modulus, G and unit weight, γ of bedrock and soil deposit are assumed as shown in **Table 2**. In Case 1, analysis is carried out by giving a displacement of 5 m to hanging wall in vertical direction. Vertical component of displacement on the surface is plotted in **Fig. 6(a),** for every 1-m

Table 1 Description of analysis

Case	Dip	Fault Type	Analysis Type
1	90	Reverse	Linear
2	45	Reverse	Linear
3	90	Reverse	Non-linear
4	45	Reverse	Non-linear
5	90	Normal	Non-linear
6	45	Normal	Non-linear

displacement of the hanging wall. From this figure, it can be understood that the hanging wall portion on the surface is lifted in proportion to the hanging

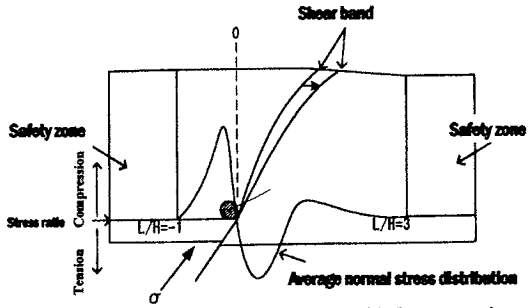

(a) From experimental results of Onizuka et al.

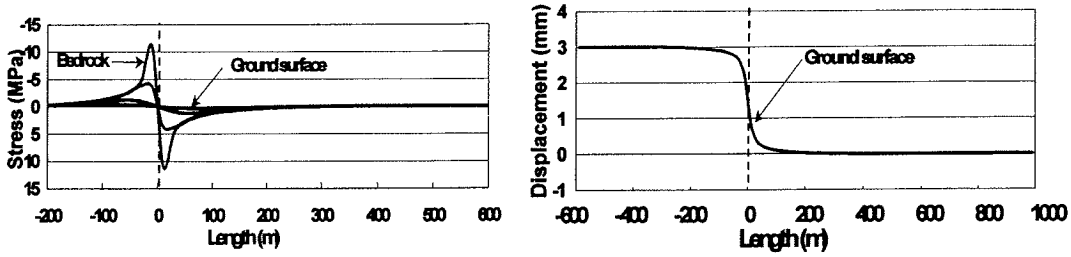

(b) From AEM

Fig. 8 Comparison with experimental results

Table 2 Material Properties

	E (kN/m^2)	G (kN/m^2)	γ (kN/m^3)
Bedrock	$66x10^6$	$33x10^6$	26.5
Soil deposit	$20x10^5$	$10x10^5$	18.0

wall displacement. **Figure 6(b)** shows stresses in vertical direction taken along the horizontal lines at different depths in soil deposit. Here stresses show high values near the central region where the underlying base fault is located. As we can see clearly from the figure, the stresses are reducing when we move near to the surface. **Figure 6(c)** shows the shear stresses in the soil deposit at regular intervals. From this figure it can be observed that the shearing stress are high near the zone of rupture and they are reducing when we move away from the rupture zone. All the shear stress curves are showing peak values at the same point, this is because of the dip angle, which is 90^0 in this case.

In Case 2, since the dip angle is 45^0, analysis is carried out by giving a displacement of 5 m to hanging wall both in vertical and horizontal directions. This means that the hanging wall is moving along the direction on dip angle i.e., 45^0. Displacement on the surface is plotted **Fig. 7(a)**, for every 1-m displacement of the hanging wall in horizontal and vertical direction. From **Fig. 7** also, it can be understood that the hanging wall portion on the surface is lifted in proportion to the hanging wall displacement. In **Fig. 7(b)**, stresses in vertical direction taken along the horizontal lines at different heights in soil deposit are plotted. Here also stresses show high values near the zone of rupture. As we can see clearly from the figure, that the stresses are reducing when we move near to the surface. **Figure 7(c)** shows the shear stresses in the soil deposit at regular intervals. From this figure it can be observed that the shearing stress are high near the zone of rupture and they are reducing when we move away from the rupture zone. However, in this case all the shear stress curves are not showing peaks at the same location. This is because of the influence of the dip angle, which is 45^0 in this case.

5. VERIFICATION OF RESULTS

To verify the accuracy of the results from the analysis, the results are compared with the results obtained by experiments conducted by Onizuka et al.[5] and the results obtained from the analytical expressions given by Okada[10].

For comparing with experimental results, model size similar to the experimental model is prepared (i.e. 1600x300 mm). This model is discritized into 1200 square elements, each of size equal to 20 mm

square. Bottom of the model is assumed as fixed boundary and right side boundary is assumed to be fixed in horizontal direction. In the bottom layer, i.e. elements at the base, first 30 elements from left side are treated as the elements to which displacement is given. Displacement of 1% of the thickness is given to these elements and the stresses inside the soil deposit are observed. **Figure 8(a)** represents the normal stresses obtained from the strain gauges fixed at the interface of bedrock and the deposit. For other details of the experiment please refer ref. 5. **Figure 8(b)** shows the results obtained by AEM analysis. From this figure it can be seen that the accuracy is comparable with the results of experiments.

For comparing with the results obtained from the analytical expressions of Okada[10], analysis is performed using the model size of 1500x150 m. Since the analytical model is for three dimensions, the 2D model is treated 3D by assuming the thickness as the third dimension. Length of the fault is 200 m and width of the fault is 150 m and the top edge of the fault is assumed to be buried at the depth of 100 m from the surface. Equations given by Okada[10] for finite rectangular source are used. A relative displacement of 5 m is given to the contacting surfaces and the deformation on the surface is observed. Figure 9(a) shows the results obtained from analytical expressions. These expressions are given for the surface displacements due to shear and tension faults in half space. Figure 9(b) shows the results obtained from the AEM analysis assuming the similar conditions. Displacement is given to the bedrock and the surface deformation is calculated for every 1m displacement. From the figures, we can easily see the agreement of the numerical results with the results of the analytical expressions. However, there is a small discrepancy in the range of influence and this is because of the difference is boundary condition. In numerical analysis boundary condition is prescribed where as in the analytical expressions, it is infinite space.

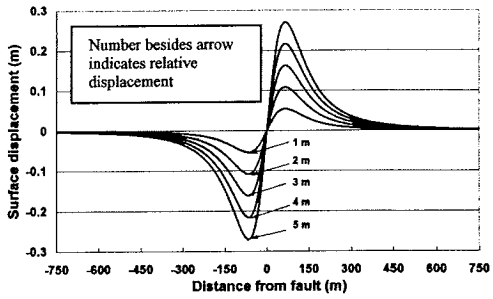

(a) From analytical expressions of Okada

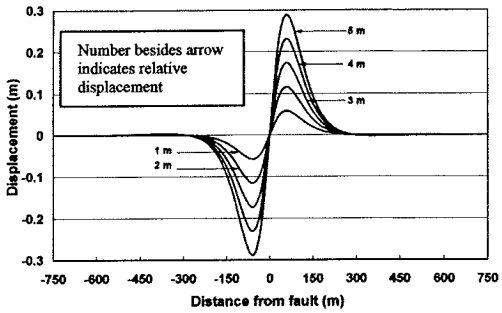

(b) From AEM

Fig. 9 Comparison with results from Analytical expressions

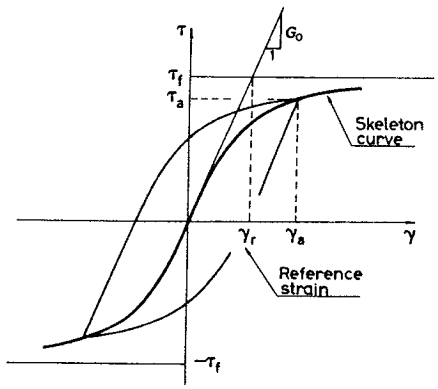

Fig. 10 Hyperbolic model

6. MATERIAL MODELING

It is logical to assume that any stress-strain curve of soils is bounded by two straight lines that are tangential to it at small strains and at large strains as shown in **Fig 10**. The tangent at small strains denoted by Go represents the elastic modulus at small strains and the horizontal asymptotic at large strain indicates the upper limit of the stress τ_f, namely the strength of soils. The stress-strain curve

$$\tau = \frac{G_o \times \gamma}{1 + \frac{\gamma}{\gamma_r}} \qquad (4)$$

for the hyperbolic model can be obtained directly from Eq. (4)

The above equation has been extensively used for representing the stress-strain relations of a variety of soils. Since the target of this paper is to

show the new application of AEM, so we adopted the simple material model which is based on only two parameters, namely, initial modulus, G_o and reference strain, γ_Γ ($=\tau_f / G_o$, where τ_f is the upper limit of the stress). However, any type of material model can be adopted by AEM. For further details on material modeling please refer ref. 7.

7. EFFECT OF ELEMENT SIZE

To discuss the effect of element size on the surface displacement and crack distribution, analyses is carried out by varying the element size. Size of the model considered for this analysis is 500x75 m. Material properties used in the analysis are shown in **Table 3**. All the properties are assumed constant and non-linear analysis is performed by changing the element size. **Figure 11** shows the comparison of vertical displacement distribution on the surface for different element sizes. From this figure, it can be clearly seen that the element size has no effect on the vertical displacement. Upon observing the crack pattern (see **Figs. 12 (a)~(d)**) for different element sizes, it can be clearly said that the element size has little to no effect.

8. NON-LINEAR ANALYSIS

Analysis is carried out for four cases. Cases 3 and 4 shown in **Figs. 13** and **14** respectively are for reverse faulting where hanging wall is moving in upward direction and the stresses in the soil deposit are compressive and the cases 5 and 6 shown in **Figs. 15** and **16** are normal faulting where the hanging wall is moving in downward direction and the stresses in the soil deposit are tensile. In the results of all the cases, displacement on the surface is plotted for every 1-m displacement of the hanging wall along the direction of dip angle i.e., 45^0. Material properties for bedrock and soil deposit in case of non-linear analysis are shown in **Table 3**.

Figures 13 (a) and **(b)** show the displacement and internal stresses for dip angle 90^0 reverse faulting respectively. From the figures, it can be observed that the displacement on the hanging wall side is in proportion to the movement of the hanging wall movement and the affected zone is concentrated near the fault region only. From **Fig. 13(b)**, it can be seen that the stresses near the zone of rupture are high and these stresses are reducing when we move towards the surface. **Figure 14 (a)** and **(b)** show surface displacement and internal stresses for dip angle 45^0 reverse faulting, respectively. From the surface displacement in **Fig. 14(a)** the effect of dip angle can be seen. Due to the change in dip angle the influence length has increased. **Figures 15 (a)** and **(b)** show the surface displacement and internal stresses for dip angle 90^0

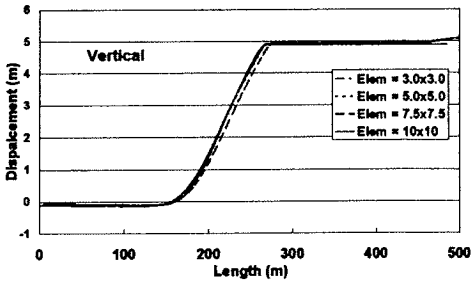

Fig. 11 Effect of element size on surface displacement

Table 3 Material Properties

	E (kN/m^2)	γ (kN/m^3)	f_c (kN/m^2)	f_t (kN/m^2)
Bedrock	$66x10^6$	26.5	$2.5x10^4$	$2.5x10^3$
Soil deposit	$20x10^5$	18.0	$1.5x10^4$	$1.5x10^3$

(a) Element size 3.0x3.0m

(b) Element size 5.0x5.0 m

(c) Element size 7.5x7.5 m

(d) Element size 10x10 m

Fig. 12 Element location and crack distribution

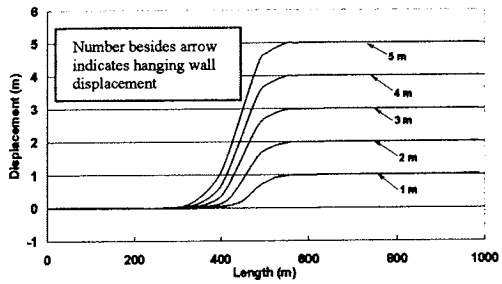

(a) Surface displacement

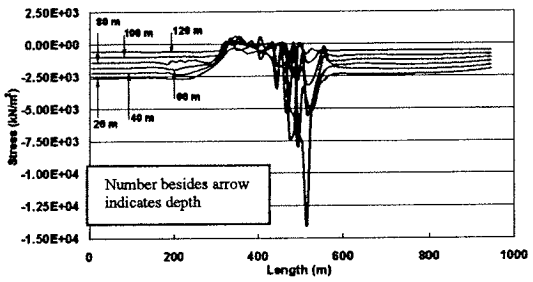

(b) Normal stresses in soil deposit at regular intervals

Fig. 13 Analysis results for Case 3

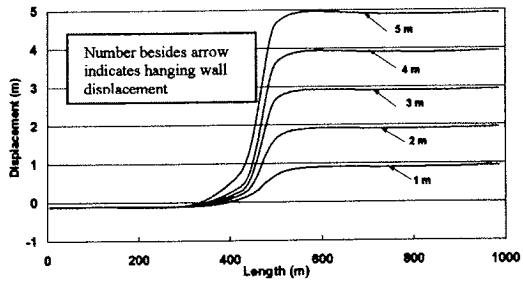

(a) Surface displacement

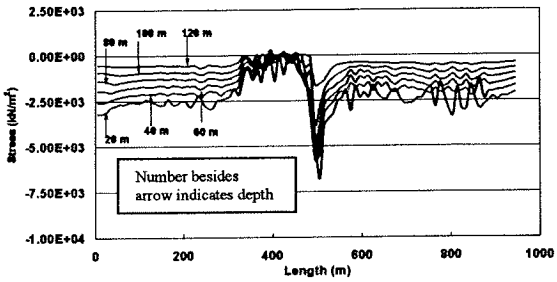

(b) Normal stresses in soil deposit at regular intervals

Fig. 14 Analysis results for Case 4

normal faulting respectively. In this case, hanging wall is moving in downward direction creating the tensile stresses in the deposit. From **Fig. 15(a)**, we can easily observe that the influence length is shorter than that in the case of reverse faulting. **Figure 15(b)** shows the stress distribution at regular intervals in soil deposit. From this figure, it is clear that the stresses are concentrated near the zone of faulting. **Figures 16 (a)** and **(b)** are similar to **Figs. 15 (a)** and **(b)** respectively, except for the case of dip angle. **Figures 17** and **18** show the elements location after the final displacement for 90^0 normal and reverse faulting respectively. From these figures, we can observe the developed rupture zone from the bedrock to the surface.

A parametric study has been carried out to show the relationship between the surface displacement and the hanging wall displacement. Vertical displacement of 5m is given to the bedrock along the direction of dip angle and the displacement at the surface is observed. **Figure 19** shows the influence length on the surface towards the left side and the right side normalized with the thickness of the soil deposit. In this figure, the solid lines are indicating the normalized surface displacement of reverse fault case and the dashed lines show the normal fault case. It is clear from the figure that the influence length on the hanging wall is increasing in case of normal fault and decreasing in case of reverse fault. And the influence length on the footwall side is decreasing in case of normal fault and increasing in case of reverse faulting.

This kind of study is necessary to establish the possible locations of the faults appearing on the surface due to future earthquakes because engineers are more concerned about the damage that might be caused when the structures are located on the vulnerable area. According to seismological point of view, some difference between the real fault and the expected fault line is acceptable but for the engineers, this difference might be sometimes of a major concern. Moreover, from the recent earthquakes, it was observed that the structures which are located very near to the zone of faulting have survived and the structures that are far have experienced major damage (JSCE (1999, a) and b)). This shows that there is a strong relation between site conditions and the dynamic characteristics of wave motion. Hence it is important to study the surface behavior based on the local soil conditions and fault characteristics. This kind of study is difficult to perform experimentally because it is difficult to prepare a model similar to actual case. On the other hand, numerical models which can predict the behavior of the media accurately in small and large deformation range and in non-linear range

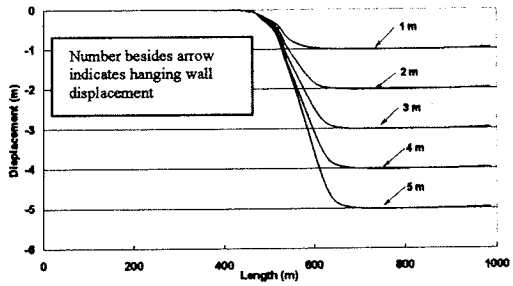

(a) Surface displacement

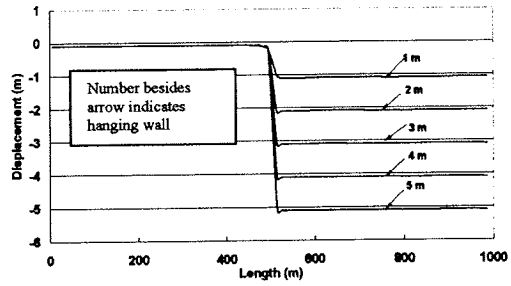

(a) Surface displacement

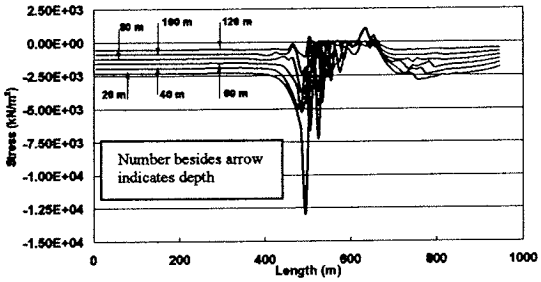

(b) Normal stresses in soil deposit at regular intervals

Fig. 15 Analysis results for Case 5

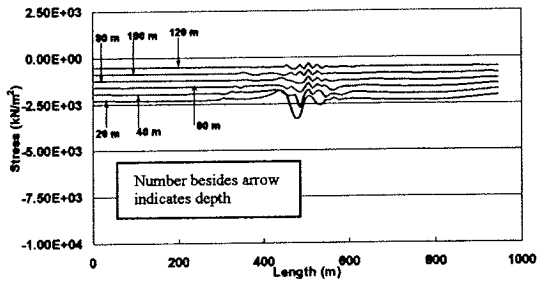

(b) Normal stresses in soil deposit at regular intervals

Fig. 16 Analysis results for Case 6

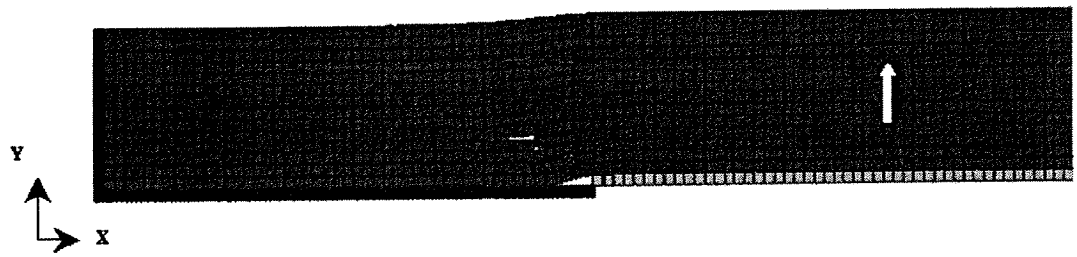

Fig. 17 Elements location after displacement (Case 3)

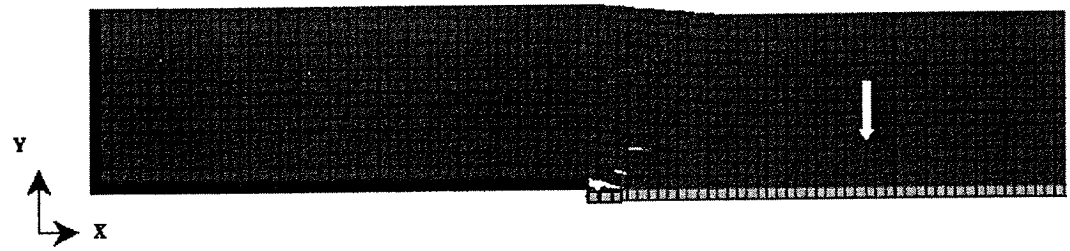

Fig. 18 Elements location after displacement (Case 5)

have the advantage of modelling any kind of soil and flexibility to change the parameters such as strength of soil, thickness of the deposit and dip angle.

9. CONCLUSIONS

A new application of Applied Element Method is proposed in this paper. A dip-slip fault zone is modelled numerically to study the influence of dip angle, bedrock displacement and the thickness of the

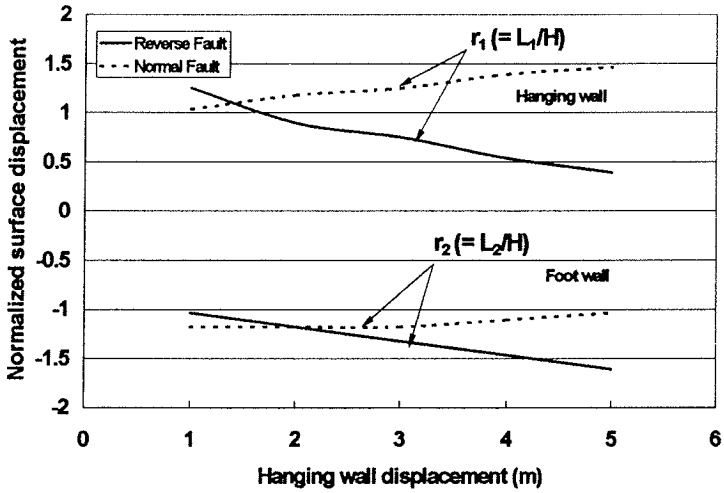

Fig. 19 Influence length on the surface

soil deposit on the length of affected zone. Since this is preliminary model, dynamic aspects such as ground motion, slip rate of fault movement, etc, are not taken into consideration. The boundary condition discussed here can be improved for qualitative discussion since there will be some movement in the horizontal direction along the boundary. Although the discussion done here is for the static case, the method can be extended to dynamic case such as modelling of the unbounded media for studying more realistic phenomenon like wave propagation and dependence on soil parameters.

REFERENCES

1) Japan Society of Civil Engineers: *The 1999 Kocaeli earthquake, Turkey, Investigation into damage to civil engineering structures*, Earthquake Engineering Committee, Japan Society of Civil Engineers, 1999 (a).
2) Japan Society of Civil Engineers: *The 1999 Ji-Ji earthquake, Taiwan, Investigation into damage to civil engineering structures*, Earthquake Engineering Committee, Japan Society of Civil Engineers, 1999 (b).
3) Cole, D. A., Jr., and Lade, P. V.: Influence zones in alluvium over dip-slip faults, *Journal of Geotechnical Engineering*, ASCE, Proc. Paper 18788, Vol. 110, No. GT5, pp. 599-615, 1984.
4) Lade, P. V., Cole, D. A., Jr. and Cummings D.: Multiple failure surfaces over dip-slip faults, *Journal of Geotechnical Engineering*, ASCE, Proc. Paper 18789, Vol. 110, No. GT5, pp. 616-627, 1984.
5) Onizuka, N., Hakuno, M. Iwashita, K. and Suzuki, T.: Deformation in grounds and bedrock stress induced by reverse dip-slip faults, *Journal of Applied Mechanics*, JSCE, Vol. 2, pp. 533-542, 1999.
6) Meguro, K. and Tagel-Din, H.: Applied element method for structural analysis: Theory and application for linear materials, *Structural Eng./Earthquake Eng.*, JSCE, Vol. 17, No. 1, 21s-35s, 2000.
7) Tagel-Din, H.: A new efficient method for nonlinear, large deformation and collapse analysis of structures, Ph.D. thesis, Civil Eng. Dept., The University of Tokyo, 1998.
8) Meguro, K. and Tagel-Din H.: A new efficient technique for fracture analysis of structures, *Bulletin of Earthquake Resistant Structure Research Center*, Institute of Industrial Science, The University of Tokyo, No. 30, 1997.
9) Wolf, J. P. and Song, Ch.: *Finite element modeling of unbounded media*, John Wiley & Sons Ltd., Baffins Lane, Chichester, England, 1996.
10) Okada, Y.: Surface deformation due to shear and tensile faults in half-space, *Bulletin of the Seismological Society of America*, Vol. 75, No. 4, pp. 1135-1154, August 1985.

(Received May 31, 2002)